HHS Public Access

Author manuscript

Biomaterials. Author manuscript; available in PMC 2022 January 24.

Published in final edited form as:

Biomaterials. 2009 February ; 30(4): 611–621. doi:10.1016/j.biomaterials.2008.09.061.

The scavenging of reactive oxygen species and the potential for cell protection by functionalized fullerene materials

Jun-Jie Yin[b,1], **Fang Lao**[a,1], **Peter P. Fu**[d], **Wayne G. Wamer**[b], **Yuliang Zhao**[a,c,*], **Paul C. Wang**[f], **Yang Qiu**[a], **Baoyun Sun**[c], **Gengmei Xing**[c], **Jinquan Dong**[c], **Xing-Jie Liang**[a,*], **Chunying Chen**[a,c,*]

[a] Division of Nanomedicine and Nanobiology, National Center for Nanoscience and Technology of China, Beijing 100190, China

[b] Center for Food Safety and Applied Nutrition, Food and Drug Administration, College Park, MD, 20740, USA

[c] Laboratory for Bio-Environmental Effects of Nanomaterials and Nanosafety, Institute of High Energy Physics, Chinese Academy of Sciences, Beijing 100049, China

[d] Division of Biochemical Toxicology, National Center for Toxicological Research, Food and Drug Administration, Jefferson, AR 72079, USA

[f] Laboratory of Molecular Imaging, Department of Radiology, Howard University, Washington DC 20060, USA

Abstract

We demonstrated that three different types of water-soluble fullerenes materials can intercept all of the major physiologically relevant ROS. $C_{60}(C(COOH)_2)_2$, $C_{60}(OH)_{22}$, and $Gd@C_{82}(OH)_{22}$ can protect cells against H_2O_2-induced oxidative damage, stabilize the mitochondrial membrane potential and reduce intracellular ROS production with the following relative potencies: $Gd@C_{82}(OH)_{22} \geq C_{60}(OH)_{22} > C_{60}(C(COOH)_2)_2$. Consistent with their cytoprotective abilities, these derivatives can scavenge the stable 2,2-diphenyl-1-picryhydrazyl radical ($DPPH^{\bullet}$), and the reactive oxygen species (ROS) superoxide radical anion ($O_2^{\bullet -}$), singlet oxygen, and hydroxyl radical ($HO^{\bullet}$), and can also efficiently inhibit lipid peroxidation *in vitro.* The observed differences in free radical scavenging capabilities support the hypothesis that both chemical properties, such as surface chemistry induced differences in electron affinity, and physical properties, such as degree of aggregation, influence the biological and biomedical activities of functionalized fullerenes. This represents the first report that different types of fullerene derivatives can scavenge all physiologically relevant ROS. The role of oxidative stress and damage in the etiology and

*Address correspondence to: Chunying Chen or Xing-Jie Liang or Yuliang Zhao, Division of Nanomedicine and Nanobiology, National Center for Nanoscience and Technology of China, Beijing 100190; and Institute of High Energy Physics, Beijing 100049, China. Email: chenchy@nanoctr.cn or liangxj@nanoctr.cn, or zhaoyuliang@ihep.ac.cn.

[1]Authors contributed equally.

progression of many diseases suggests that these fullerene derivatives may be valuable in vivo cytoprotective and therapeutic agents.

Keywords

Gadolinium endohedral metallofullerenol; fullerenol; carboxyfullerene; scavenging activity; cytoprotection; reactive oxygen species

1. Introduction

A large number of *in vitro* and *in vivo* studies suggest that oxidative stress is linked to either the primary or secondary mechanisms of progression for many acute and chronic diseases. As mediators of oxidative stress, reactive oxygen species (ROS), which include superoxide radical anion ($O_2^{\bullet -}$), hydroxyl radical ($HO^{\bullet}$), singlet oxygen ($^1O_2$), and hydrogen peroxide, have been implicated in the etiology of several human diseases, including amyotrophic lateral sclerosis, arthritis, cancer, cardiovascular disease, and a number of neurodegenerative disorders [1, 2]. Cellular targets of ROS include DNA, proteins and lipids. Damage to these cellular targets has been associated with aging and several human diseases including cancer, athereosclerosis, ischemia, inflammation, and liver injury [3–5]. In addition, it has been determined that compared to normal cells, cancer cells are under increased oxidative stress, which is associated with increased generation of ROS and can result in stimulation of cellular proliferation, mutations, and genetic instability [6–8]. Thus, chemical species that potently scavenge ROS may be of great significance in biomedicine both for maintaining health and for use in cancer chemotherapy.

It is well established that fullerenes and their derivatives possess a unique capacity for scavenging ROS [9–11]. Because underivatized fullerenes are insoluble in water and biological systems, hydroxylated and other derivatized fullerenes have been utilized due to their increased water solubility and resulting increase in payload of ROS-scavening activity to target cells and tissues. Demonstrated protective effects of water-soluble fullerene derivatives include reduction of injury on ischemic reperfusion of the intestine [10], a decrease in numbers of cells undergoing apoptosis [11], reduction in free radical levels in organ perfusate [12], and neuroprotective effects [13].

Hydroxylated fullerenes (fullerenols) and malonic acid-substituted fullerenes (carboxyfullerenes) are two major groups in water-soluble fullerene materials, which were found to possess biological significance as free radical scavengers [9–15]. For example, Dugan et al. [14–15] demonstrated that carboxylic acid-substituted C_{60} derivatives had potent ROS-scavenging activity. These fullerene derivatives prevented apoptosis of cultured cortical neurons induced by exposure to N-methyl D-aspartate (NMDA)-agonists, protected the nigrostriatal dopaminergic system from iron-induced oxidative injury, and showed effective neuroprotective antioxidant activity *in vitro* and *in vivo*. Fullerenols have also been demonstrated to be particularly valuable candidates for use as free radical scavengers or water-soluble antioxidants in biological systems [16].

Endohedral metallofullerenes, i.e., compounds in which a fullerene encapsulates a metal atom(s), have shown great promise for use in biomedical science. Although C_{60} has been the most commonly studied fullerene in biological systems, few endohedral materials have been synthesized using C_{60} as a cage molecule because of the limited interior volume of C_{60}. Therefore, most endohedral metallofullerenes are synthesized using C_{82} or higher molecular weight fullerenes, and many derivatives of C_{82} fullerenes have been synthesized in our laboratory. Gd@C_{82} is one of the most important molecules in the metallofullerene family [17]. Gadolinium endohedral metallofullerenol (e.g., Gd@$C_{82}(OH)_{22}$) is a functionalized fullerene with gadolinium, a transition metal in the lanthanide family, trapped inside the C_{82} fullerene cage. We have previously reported that the chemical and physical properties of gadolinium endohedral metallofullerenols are dependent on the number and position of the hydroxyl groups on the fullerene cage [17]. These results demonstrated that modifying the outer cage of Gd@C_{82} with a number of hydroxyl groups tunes the electronic properties of the inner metal atom as well as the electron density and polarizability of the electrons at the fullerene's surface.

Gadolinium endohedral metallofullerenols were originally designed as magnetic resonance imaging (MRI) contrast agents for biomedical imaging [18]. These materials have additionally attracted attention due to their potential use in chemotherapy [18, 19]. We have recently reported that aggregates of Gd@$C_{82}(OH)_{22}$, i.e., Gd@$C_{82}(OH)_{22}$ nanoparticles, inhibited the proliferation of tumors and decreased the induction of antioxidant defenses *in vivo* [18, 19]. We have also determined that intraperitoneally injected $[Gd@C_{82}(OH)_{22}]_n$ nanoparticles efficiently inhibited the growth of hepatoma cells implanted into the legs of mice and that inhibition of tumor growth involved reduction in tumor-induced oxidative stress rather than direct cytotoxicity to tumor cells [19]. However, the molecular mechanisms underlying these protective effects are still unclear.

It has been shown that a number of fullerenes, fullerenols, and endohedral metallofullerenols are capable of reacting with and/or scavenging free radicals [15, 16, 20]. However, much less is known about the protective role of Gd@$C_{82}(OH)_{22}$ nanoparticles. It has not been determined if the ROS scavenging capability of $[Gd@C_{82}(OH)_{22}]_n$ nanoparticles is higher than the other functionalized fullerenes (e.g., functionalized C_{60}-fullerenols and C_{60}-carboxyfullerenes). In this study we employ the electron spin resonance (ESR) spin trap technique to provide direct *in vitro* evidence that Gd@$C_{82}(OH)_{22}$, a fullerenol ($C_{60}(OH)_{22}$), and a carboxyfullerene ($C_{60}(C(COOH)_2)_2$), can efficiently scavenge different types of free radicals and inhibit lipid peroxidation. Both ROS, i.e. superoxide radical anion ($O_2^{\bullet -}$), hydroxyl radical ($HO^{\bullet}$) and singlet oxygen ($^1O_2$) as well as the stable, nitrogen-centered free radical, $DPPH^{\bullet}$ were intercepted by these fullerene derivatives. Using human lung adenocarcinoma A549 cells or rat brain capillary endothelial cells (rBCECs), we further demonstrate that these fullerene derivatives reduce H_2O_2-induced cytotoxicity, free radical formation and mitochondrial damage.

2. Materials and Methods

2.1. Preparation and Characterization of Water-soluble Fullerene Derivatives

Highly purified hydroxylated and malonic acid substituted derivatives of C_{60} were prepared by previously published methods [21, 22]. Although the diameter of an isolated C_{60} molecule is about 0.7 nm, fullerene derivatives readily aggregate and form nanoparticles in aqueous solution. Additional physical and chemical properties of $C_{60}(OH)_{22}$ and $C_{60}(C(COOH)_2)_2$ can be found in the previous reports [21, 22]. The synthesis and characterization of $Gd@C_{82}(OH)_{22}$ have been previously described [18]. The nanoparticles' sizes were characterized in water using a field emission scanning electron microscope (FE-SEM, Hitachi S-4800, Japan). To investigate their particle sizes in the matrix used for ESR studies, we additionally measured their particle size distribution in phosphate buffered saline (PBS, 20 mM phosphate, 0.8% NaCl, pH 7.4) using dynamic light scattering (DLS) (Nano ZS90, Malvern). The DLS data were in agreement with those obtained by SEM (data not shown).

The fullerene derivatives used for ESR detection were prepared according to the experimental requirements (see Materials and Methods below). For cell experiments, nanoparticles of fullerene derivatives were diluted as needed with PBS prior to use. We further compared the spectra of different fullerenes, which were recorded between 200 nm and 600 nm using a UV-Vis spectrophotometer (CARY 100 Bio, Varian, Inc., USA) at room temperature of 20–25 °C.

2.2. Reagents

Hydrogen peroxide (H_2O_2), xanthine, diethylenetriaminepentaacetic acid (DTPA), 1, 1-diphenyl-2-picrylhydrazyl radical ($DPPH^{\bullet}$) and 2,2,6,6-tetramethyl-4-piperidone (TEMP) were purchased from Sigma Aldrich (St. Louis, MO) 5-tert-Butoxycarbonyl-5-methyl-1-pyrroline-N-oxide (BMPO) and 5-diethoxyphosphoryl-5-methyl-I-pyrroline N-oxide (DEPMPO) were supplied by Oxis International (Portland, OR). Basic endothelial cell growth factor (bECGF) and xanthine oxidase were obtained from Roche Applied Science (Indianapolis, IN). Egg phosphatidylcholine was obtained from Avanti Polar Lipids, Inc. (Alabaster, AL). 2,2′-Azobis(2-amidinopropane) dihydrochloride (AAPH) was purchased from Wako Chemicals (Richmond, VA). All reagents used in cell culture were obtained from HyClone Co. (Logan, UT) unless otherwise stated. Fluorescent probes JC-1 (5, 5′, 6, 6′-tetrachloro-1, 1′, 3, 3′–tetraethylbenzimida-zolylcarbocyanine iodide) and CM-H2DCFDA (5-(and-6)-chloromethyl-2′, 7′-dichlorodihydrofluorescein diacetate, acetyl ester) were purchased from Invitrogen Co. (Molecular Probes, Eugene, OR). All other reagents used were at least of analytical grade.

2.3. Cell cultures

Primary brain capillary endothelial cells (rBCEC) were prepared following a modified protocol of Deli et al. [23]. In brief, four Wistar rats (85–90g) were sacrificed by cervical dislocation, the forebrains were collected, meninges were removed and the grey matter was minced and digested with type □ collagenase. The cell pellets was resuspended in Dulbecco's modified Eagle's medium (DMEM) and centrifuged at 1500 rpm for 5

minutes. After three cycles of suspension and centrifugation, the pellet containing capillary endothelial cells was collected and cultured in DMEM medium with 20% fetal bovine serum (FBS), supplemented with 10 U/mL heparin (Sigma-Aldrich Co., St. Louis, MO), 100 U/mL penicillin-streptomycin solution and 150 μg/mL endothelial cell growth factor (bECGF). All experiments used rBCEC cells in the third passage. A549 cells from the American Type Culture Collection (ATCC) (Manassas, VA) were maintained in DMEM supplemented with 10% FBS and antibiotics (100 U/mL, penicillin-streptomycin) at 37 °C in 5% CO_2. Experiments were performed at least 3 times.

2.4. Cell viability assessment

The activity of mitochondrial dehydrogenase, a critical measure of mitochondrial function, and cellular toxicity, was determined according to a protocol previously described. Briefly, rBCECs or A549 cells at 90% confluence were cultured with different concentrations of fullerene derivative nanoparticles (10, 50, 100 μM) for 24 h. The medium was then replaced with fresh medium containing 50 μM H_2O_2 (Chemical Reagents Co., Beijing). After treatment with H_2O_2 for 2 h, cells were washed three times with PBS. The mitochondria's ability to reduce a tetrazolium salt to a formazan dye was used to assess mitochondrial dehydrogenase activity. Briefly, a certain volume of solution containing tetrazolium salt (available in the CCK-8 Kit from Dojindo Laboratories, Japan) was added to the culture medium. After incubation for 1.5 h at 37°C, the absorbance at 450 nm was read using a Bio-Rad 680 microplate reader (Bio-Rad, Hercules, CA). Measurement for each treatment was repeated in triplicate.

2.5. Measurement of Mitochondrial Membrane Potential

The fluorescent potentiometric dye JC-1 is a cationic carbocyanine compound that accumulates in mitochondria and can be used to measure the mitochondrial membrane potential ($\Delta\psi_m$). In intact cells, JC-1 accumulates in the mitochondria as aggregates and exhibits a fluorescence emission shift from green (~525nm), the monomeric form, to red (~600 nm), the aggregate. When viewed under a fluorescence microscope, JC-1 is seen as a green monomer in the cytosol and as a red aggregate in respiring mitochondria. Mitochondrial damage is measured as a reduction in $\Delta\psi_m$, i.e. a decrease in the red/green fluorescence ratio.

A549 or rBCECs cells (1.0×10^5 cells/ml), treated with fullerene derivative nanoparticles and H_2O_2 as described above, were labeled with 3 μM JC-1 for 20 min in a 37°C incubator (5% CO_2). After cells were washed three times with PBS, the fluorescence was detected using a laser confocal scanning microscope (Olympus FV 500). The JC-1 monomer was detected at a 530 nm emission wavelength. The fluorescence of the JC-1 aggregate was measured at 590 nm emission. The cells were also stained with Hoechst 33258 to show the nuclei as blue. Cells treated with H_2O_2 only were used as the positive control.

2.6. Measurement of Intracellular ROS Concentration

CM-H_2DCFDA was used to measure intracellular ROS production as previously reported [24]. A549 or rBCECs cells were treated with fullerene derivative nanoparticles and H_2O_2 as described above for measurement of mitochondrial dehydrogenase activity. After

treatment, the samples were incubated with 5 μM CM-H_2DCFDA at 37°C for 30 minutes in the dark, washed three times with PBS, and then analyzed using a FACSCalibur flow cytometer (Becton Dickinson, San Jose, CA). The 488-nm excitation and 515-nm emission wavelengths were used to measure the fluorescence intensity of CM-H_2DCFDA. Negative controls (without 50 μM H_2O_2 and 100 μM nanoparticles) and positive controls (with 50 μM H_2O_2 and without nanoparticles) were included in the treatment groups with 100 μM nanoparticles. Data are representative of three experiments.

2.7. Electron Spin Resonance (ESR) Spectroscopic Measurements

All ESR measurements were carried out at ambient temperature (27°C) using a Varian E-109 X-Band ESR Spectrometer (Varian Inc., Palo Alto, CA). To analyze the free radical scavenging capability of fullerene derivatives, cell-free radical producing systems were used for measurement of DPPH•, superoxide radical anion, hydroxyl radical and singlet oxygen. In addition, lipid peroxidation was measured using a cell-free, *in vitro* system.. The concentration of fullerene derivatives nanoparticles was varied in order to determine the maximal scavenging efficacy for each radical studied. Each experiment was repeated at least three times.

2.8. DPPH• Scavenging Activity

DPPH• is a stable, nitrogen-centered free radical. While DPPH• has no involvement in physiological processes, attenuation of the ESR signal for DPPH• is one of the methods widely used to demonstrate a chemical's ability to scavenge free radicals through donation of a hydrogen atom or, in some cases, electron transfer [25]. The effect of each fullerene derivative on the ESR spectrum of DPPH• was examined. All samples contained 100 μM DPPH• in a mixture of 20% ethanol in PBS. To examine scavenging ot DPPH•, samples also contained 100 μM of the selected fullerene derivative. ESR spectra were recorded 5 min after addition of the fullerene derivative. Spectra were obtained using 15 mW incident microwave power and 100 kHz field modulation of 2 G. The scavenging effect was determined by comparison with a control group lacking nanoparticles.

2.9. Superoxide Radical Anion ($O_2^{\bullet -}$) Scavenging Activity

BMPO was used to trap and detect $O_2^{\bullet -}$ by ESR spectroscopy. Superoxide radical anion was generated using the xanthine/xanthine oxidase system. The scavenger-radical reaction was initiated by addition of xanthine oxidase solution (XOD). The reaction contained 100 μM xanthine, 20 mM BMPO, 50 μM DTPA, 0.1 U/mL XOD and 150 μM of a fullerene derivative. The ESR spectra were recorded at 1.5 min after initiating the generation of $O_2^{\bullet -}$ by addition of XOD. The following instrument settings were used for collecting ESR spectra: microwave power of 10 mW, field modulation frequency of 100 kHz, and modulation amplitude of 1 G.

2.10. Hydroxyl Radical (HO•) Scavenging Activity

Interception of hydroxyl radicals by each fullerene derivative was determined by the ESR spin-trapping technique [26]. The ESR assay was based on the competition between the trapping agent, DEPMPO, and the fullerene derivative nanoparticles for HO•. Hydroxyl

radicals were generated by the classical Fenton reaction with the reaction mixture containing freshly prepared 500 μM DEPMPO, 20 μM $FeSO_4$ (1000 μM stock solution, freshly made) and 200 μM H_2O_2 with or without 100 μM of a fullerene derivative. The ESRdata were collected at ambient temperature, 2 min after initiating the formation of $HO^{\bullet}$ by addition of $FeSO_4$. Spectra were recorded using the same spectrometer settings as those used for detecting $O_2^{\bullet -}$.

2.11. Singlet Oxygen ($^1O_2$) Scavenging Activity

The spin trap TEMP was used to determine the three nanoparticles' abilities to scavenge $^1O_2$. Singlet oxygen was generated by photoexcitation of Rose Bengal at 560 nm. ESR data were collected for samples containing 10 mM TEMP and 0.1 mM Rose Bengal with or without fullerene nanoparticles (0.2 mM). Samples were irradiated at ambient temperature in the ESR microwave cavity using a 1 K watt xenon lamp (Schoeffel, Kratos Inc., Westwood, NJ) with a single monochromator (GM 252, Shoeffel, Kratos Inc., Westwood, NJ) set at 560 nm. The instrument settings for obtaining ESR spectra of the TEMP-$^1O_2$ adduct were: 15 mW microwave power and 1 G field modulation. The time dependence of the ESR signal for the formation of the TEMP-$^1O_2$ adduct was measured using the time dependent intensity of the center line of the ESR spectrum during irradiation of the sample (typically 30 min.).

2.12. Inhibition of Lipid Peroxidation

The effects of fullerene derivatives on peroxidation of lipids in liposomes were measured using ESR oximetry. The ESR oximetry measurement is based on changes in the relaxation time of the spin probe due to the bimolecular collision of O_2 with the spin probe. Because O_2 is paramagnetic, this collision results in spin exchange between O_2 and the spin probe, resulting in shorter relaxation times (both T_1 and T_2). Consequently, at higher concentrations of dissolved O_2, broader ESR signals are observed for the spin probe [27]. Since the integrated area of the ESR signal over the scanning range is unaffected by these effects on the relaxation times, broadening of the spin probe's ESR signal is necessarily accompanied by a decrease in the peak height of the ESR signal. This can be readily seen for the ESR signal measured for ^{15}N-Tempone (^{15}N-PDT) under N_2 and O_2 atmospheres (Figure 7A). When the ESR signal is measured under a N2 atmosphere, a narrower, line width and higher peak intensity is observed compared to measurement of the ESR signal under an O_2 atmosphere. Under conditions where the levels of dissolved O_2 vary, a time dependent decrease in line width and increase in the peak intensity of the ESR signal indicate continuous O_2 consumption.

Liposomes were prepared as previously described [27]. Briefly, a suspension of 30 mg/mL egg PC liposomes, 0.1 mM ^{15}N-Tempone (^{15}N-PDT) with or without fullerene derivatives (0.2 mM $Gd@C_{82}(OH)_{22}$, 0.2 mM $C_{60}(OH)_{22}$ or 0.3 mM $C_{60}(C(COOH)_2)_2$) was added to a capillary tube. The lipid peroxidation was initiated by adding 25 mM AAPH, which is known to strongly induce lipid peroxidation in cellular and reconstituted membranes [26]. The capillary tube was then sealed and positioned in the ESR instrument. ESR spectra were then recorded at 4 min intervals for 24 min. Signals were obtained with a 1 G scanning width, 1 mW incident microwave power and with 100 KHz field modulation. All ESR spectra were recorded at the low field line of ^{15}N-Tempone (^{15}N-PDT) and at 37°C.

2.13. Statistical analysis

All data are expressed as the mean ± S.D. For analysis of results from studies on cultured cells, the unpaired Student's *t* test was applied to identify significant differences between the groups treated with fullerene derivatives and non-treated as controls. For the ESR experiments, a one-way analysis of variance (ANOVA) followed by a *post hoc* Fisher protected least-significant-difference test was applied. $P < 0.05$ was considered to be a significant difference.

3. Results

3.1 Characterizations

Prior to studies on the scavenging of ROS, field emission scanning electron microscopy (FE-SEM) was employed for characterization of $Gd@C_{82}(OH)_{22}$, $C_{60}(OH)_{22}$, and $C_{60}(C(COOH)_2)_2$ in PBS solution (Fig. 1). These fullerene derivatives readily aggregate and form nanoparticles in aqueous solution. To further investigate their particle sizes in the matrix used for biological experiments and ESR studies, we measured their size distribution in physiological saline using dynamic light scattering (DLS). The DLS data closely match with those obtained by SEM. The average diameter of $Gd@C_{82}(OH)_{22}$, $C_{60}(OH)_{22}$, and $C_{60}(C(COOH)_2)_2$ nanoparticles determined by DLS are 78±5.3, 123±14.2, and 170±14.7 nm, respectively. Thus, nanoparticles formed from fullerenol encapsulating Gd (i.e. $Gd@C_{82}(OH)_{22}$) are significantly smaller than nanoparticles from metal-free fullerenes (i.e. $C_{60}(OH)_{22}$, and $C_{60}(C(COOH)_2)_2$). As seen in Fig. 1, the UV-Vis spectra of hydroxylated fullerenes ($Gd@C_{82}(OH)_{22}$ and $C_{60}(OH)_{22}$) differ significantly from the spectra of $Gd@C_{82}$ and C_{60}. C_{60} exhibits a marked absorption band with a maximum at 340 nm, while $Gd@C_{82}$ shows an obvious shoulder at 310–330 nm. Concentration dependent changes in the DLS data (data not shown) and UV spectroscopy of aqueous solutions of these water-soluble fullerenes revealed evidence of the formation of aggregates or clusters at the concentration of 200 μM.

3.2. Protective Effect against Cellular Oxidative Stress

The protective effects of water-soluble fullerene derivatives were investigated using two cellular systems. Treatment of adenocarcinoma (A549) cells or rat brain capillary endothelial cells (rBCEC) with 50 μM H_2O_2 for 2 hr resulted in significant cellular toxicity, measured as loss of mitochondrial dehydrogenase activity (Fig. 2). Pre-treatment with fullerene derivatives, 24 h prior to addition of H_2O_2, resulted in protection against cellular toxicity (Fig. 2). Concentration dependent protection against cytotoxicity was observed following treatment with each of the fullerene derivatives. The protective effects of the fullerenes against cytotoxicity are further summarized in Table 1. As shown in Fig. 2 and summarized in Table 1, $Gd@C_{82}(OH)_{22}$ nanoparticles exhibit the greatest protective effects against H_2O_2-induced cytototoxicity, followed by $C_{60}(OH)_{22}$ nanoparticles, with $C_{60}(C(COOH)_2)_2$ nanoparticles the least protective.

The fullerene derivatives were also evaluated for their ability to protect against H_2O_2-induced mitochondrial damage measured as a reduction in the mitochondrial membrane potential ($\Delta\psi_m$). In cells untreated with H_2O_2, the JC-1 probe was seen primarily as red

aggregates, indicating substantial uptake by respiring mitochondria (Fig. 3A). For both rBCEC and A549 cells, treatment with 50 μM H_2O_2 for 2 h resulted in a decrease in red aggregates of the JC-1 probe in mitochondria and an increase in green monomers of the JC-1 probe in the cytoplasm (Fig. 3B). This result demonstrates H_2O_2-induced mitochondrial damage and a reduction in $\Delta\psi_m$. Samples pre-treated with 100 μmol/L $C_{60}(C(COOH)_2)_2$, $C_{60}(OH)_{22}$, and $Gd@C_{82}(OH)_{22}$ demonstrate an increase in red fluorescence compared to the untreated. Pretreating cells with $Gd@C_{82}(OH)_{22}$ nanoparticles (Fig. 3E) resulted in partial restoration of mitochondrial uptake of the JC-1. The restoration of mitochondrial uptake observed following pretreatment with $Gd@C_{82}(OH)_{22}$ was higher than that observed following pretreatment with $C_{60}(C(COOH)_2)_2$ (Fig. 3C) or $C_{60}(OH)_{22}$ (Fig. 3D). This result indicates that $Gd@C_{82}(OH)_{22}$ protects against oxidative injury to cellular mitochondria better than $C_{60}(C(COOH)_2)_2$ and $C_{60}(OH)_{22}$ fullerene derivatives.

The total intracellular levels of ROS, resulting from treatment of cells with 50 μM H_2O_2 for 2 h, was measured by flow cytometry in A549 cells and rBCECs cells labeled with CM-H_2DCFDA. Figure 4 shows the effects of $C_{60}(C(COOH)_2)_2$, $C_{60}(OH)_{22}$, and $Gd@C_{82}(OH)_{22}$ nanoparticles on the levels of H_2O_2–induced intracellular ROS. Treatment of rBCEC or A549 cells with H_2O_2 resulted in a significant increase in intracellular ROS. Pretreatment with nanoparticles of fullerene derivatives significantly reduced the levels of H_2O_2–induced ROS in both cell types. Pretreatment with $Gd@C_{82}(OH)_{22}$ or $C_{60}(OH)_{22}$ nanoparticles resulted in greater reduction of H_2O_2–induced intracellular ROS levels than pretreatment with $C_{60}(C(COOH)_2)_2$ nanoparticles (Fig. 4 and Table 1). The effects of three fullerene derivatives on levels of intracellular ROS are further summarized in Table 1. The results shown in Table 1 demonstrate a correlation between the cellular protective effects of fullerene derivatives and their ability to scavenge intracellular ROS. Hydroxylated fullerenols were stronger ROS scavenger than malonic acid derivatives.

3.3. DPPH• Radical-Scavenging Activities

To determine whether or not these fullerene derivatives can scavenge nitrogen-centered radicals, experiments were performed using the stable, nitrogen-centered free radical, DPPH•. The effects of the three water-soluble fullerene derivatives on the ESR spectra of DPPH• are shown in Figure 5A. A characteristic one-line spectrum was obtained for solutions of 100 μM DPPH• in 20% ethanol. A reduction in signal intensity was associated with the addition of any of the three fullerene derivatives. However, the radical-scavenging activity of the fullerene derivatives differed. $Gd@C_{82}(OH)_{22}$ was significantly more efficient in quenching DPPH• than $C_{60}(OH)_{22}$. $C_{60}(C(COOH)_2)_2$ had the weakest ability in scavenging DPPH•. All fullerenes were present at a concentration of 100 μM. The inhibitory effects of three fullerene derivatives are further summarized in Table 2. As shown in Fig. 5 and summarized in Table 2, $Gd@C_{82}(OH)_{22}$ nanoparticles exhibit the highest capability to eliminate DPPH• radical, followed by $C_{60}(OH)_{22}$ nanoparticles, with $C_{60}(C(COOH)_2)_2$ nanoparticles the least effective ($P<0.05$).

3.4. Superoxide Radical Anion ($O_2^{\bullet -}$) Scavenging Capability

The relative scavenging abilities of the fullerene derivatives for $O_2^{\bullet -}$, generated by the xanthine/xanthine oxidase system, are seen in Fig. 5B. The typical ESR spectrum for the

spin adduct between $O_2^{\bullet -}$ and the spin trap, BMPO, was observed. All of the fullerene derivatives, at a final concentration of 150 μM, reduced the spin adduct's signal intensity. The relative scavenging abilities of the fullerenes for $O_2^{\bullet -}$ were similar to those observed for scavenging of DPPH$^{\bullet}$, i.e., $Gd@C_{82}(OH)_{22} \approx C_{60}(OH)_{22} > C_{60}(C(COOH)_2)_2$. The inhibitory effects of three fullerene derivatives are further summarized in Table 2.

3.5. Hydroxyl Radical (HO$^{\bullet}$) Scavenging Capability

Hydroxyl radicals were generated by the classical Fenton reaction involving the reaction of $FeSO_4$ and H_2O_2 [29]. The Fenton reaction was started by the addition of Fe(II) (200 μM final concentration), 200 μM H_2O_2 and 500 μM DEPMPO. The signal intensity of the spin adduct was reduced by addition of each fullerene derivative at a final concentration of 100 μM (Fig. 5C). The relative efficiencies for quenching the HO$^{\bullet}$ were similar to those observed for quenching DPPH$^{\bullet}$ and $O_2^{\bullet -}$. Reductions in signal intensities were approximately 55%, 67% and 88% for $C_{60}(C(COOH)_2)_2$, $C_{60}(OH)_{22}$ and $Gd@C_{82}(OH)_{22}$, respectively. The inhibitory effects of three fullerene derivatives are further summarized in Table 2.

3.6. Singlet Oxygen ($^1O_2$) Scavenging Activity

The spin trap TEMP was used to demonstrate the ability of $Gd@C_{82}(OH)_{22}$, $C_{60}(OH)_{22}$, and $C_{60}(C(COOH)_2)_2$ to scavenge $^1O_2$. These three fullerene derivatives exhibit UV-Visible spectral absorption in the range of 200–350 nm (Fig. 1D). To avoid photoexcitation of these compounds, singlet oxygen was generated by irradiation of Rose Bengal at 560 nm for 30 min. In the presence of TEMP, the ESR signal of TEMPO adduct was observed (Fig. 6). The ESR signal of TEMPO adduct intensity was reduced by addition of each of the fullerene derivatives (Fig. 6). Again, $Gd@C_{60}(OH)_{22}$ showed the strongest inhibition and $C_{60}(C(COOH)_2)_2$ exhibited the least. The efficiencies of $C_{60}(C(COOH)_2)_2$, $C_{60}(OH)_{22}$ and $Gd@C_{82}(OH)_{22}$ in inhibiting formation of TEMPO are 9.1%, 38.2%, and 58.2%, respectively (Table 2).

3.7. Inhibition of Lipid Peroxidation in Liposomes

2,2′-Azobis(2-amidinopropane) dihydrochloride (AAPH) is a strong inducer of lipid peroxidation [27]. The impact of radical scavenging activity by the fullerene nanoparticles was further examined by measuring the ability of fullerene nanoparticles to inhibit lipid peroxidation induced by AAPH. Free radicals, generated through the decomposition of AAPH, produce a time dependent peroxidation of polyunsaturated lipids in liposomes. Using ESR oximetry, the consumption of oxygen accompanying lipid peroxidation is measured as a time dependent narrowing of the ESR signal for the spin probe, ^{15}N-Tempone. Since the area beneath the signal intensity *vs.* magnetic field curve remains constant, this narrowing of the ESR signal is necessarily accompanied by an increase in the peak height of the ESR signal within the scanning range (Fig. 7A). 25000 μM AAPH was added to initiate the lipid peroxidation. The control sample, with egg PC alone, showed a sharp spectral peak for ^{15}N-Tempone, while addition of fullerene derivatives resulted in lower consumption rates of oxygen seen as smaller peak heights in the ESR signal due to lower rates of line narrowing of the spin probe. Addition of $Gd@C_{82}(OH)_{22}$ (Fig. 7B) resulted in strongest inhibition of lipid peroxidation measured as retardation of line narrowing, and corresponding retardation in the growth of the ESR signal's intensity,

compared to $C_{60}(C(COOH)_2)_2$ and $C_{60}(OH)_{22}$ (Fig. 7B). The inhibitory effects of three fullerene derivatives on lipid peroxidation are further summarized in Table 2.

4. Discussion

In this study we employ ESR techniques to systematically provide direct evidence that $Gd@C_{82}(OH)_{22}$, $C_{60}(OH)_{22}$, and $C_{60}(C(COOH)_2)_2$ nanoparticles can effectively scavenge different types of free radicals/ROS. This represents the first report that several different types of fullerene derivatives can scavenge all physiologically relevant ROS. Consistent with these results, we also determined that these fullerene derivatives can inhibit lipid peroxidation. Our study also shows that these nanoparticles protect human lung adenocarcinoma (A549) cells and normal rat brain capillary endothelial (rBCEC) cells against H_2O_2-induced cytotoxicity (Figs. 2–4).

In contrast to water-soluble C_{60} derivatives, nanoparticles of underivatized C_{60} appear to lack significant cytoprotective properties. Indeed, investigators have shown that underivatized C_{60} can elicit cytotoxicity, the formation of ROS and lipid peroxidation [30–34]. Sayes *et al.* have reported that aqueous suspensions containing nanoparticles of underivatized C_{60} are cytotoxic to human dermal fibroblasts at low levels (LC_{50} = 20 ppb) and can generate ROS such as $O_2^{\bullet}$ [33]. Sayes *et al.* have also observed that the cytotoxicity of underivatized C_{60} is associated with lipid peroxidation [33]. It is noteworthy that derivatization of the fullerene cage with carboxyl and hydroxyl groups results in a dramatic decrease in the cytotoxicity and generation of ROS [33, 34].

We have demonstrated that Gd-encaged fullerenes are much stronger ROS scavenger than hollow fullerenes, though they all can intercept all of the major physiologically relevant ROS. These radical scavenging abilities of fullerenes may be attributed to several molecular properties. Foremost is the large electron affinity of fullerenes. The electron affinity of C_{60} has been reported to be 2.7 eV while the larger fullerene, C_{82}, has an electron affinity of 3.14 eV [35,36]. Insertion of Gd into the C_{82} fullerene further increases the electron affinity. Boltalina *et al.* have measured the electron affinity of $Gd@C_{82}$ to be 3.3 ± 0.1 eV [35]. Differences in electron affinities may contribute to the relative efficiencies ($Gd@C_{82}(OH)_{22} > C_{60}(OH)_{22} > C_{60}(C(COOH)_2)_2$) which we observe for radical scavenging and cytoprotection. Adding to the effects of electron affinity is the large polarizability of fullerenes, which further facilitates attachment of electrons and radicals to the nanosurface of fullerenes [37]. A second factor contributing to broad-based radical scavenging activity is derivatization of the fullerene's nanosurface. Ali *et al.* have demonstrated that derivatizing a C_{60} fullerene with *tris*-malonic acid results in electron deficient areas on the fullerene's surface which facilitates binding of $O_2^{\bullet -}$ [38]. Binding of a second $O_2^{\bullet -}$ to an adjacent electron deficient area results in destruction of $O_2^{\bullet -}$ production of H_2O_2 and regeneration of the fullerene in a reaction similar to that catalyzed by superoxide dismutase. Derivatizing with hydroxyl groups similarly induces electron deficient areas on the fullerene's surface and may lead to similar catalytic activity for polyhydroxylated fullerenes such as $[Gd@C_{82}(OH)_{22}]_n$. Indeed, the potent scavenging of $O_2^{\bullet -}$ that we and other investigators have observed strongly suggests that polyhydroxylated fullerenes posses a superoxide dismutase activity [16,38]. A similar catalytic sequence of

events appears to result in scavenging of $^1O_2$ by fullerenes. Although fullerenes are not good substrates for oxidation by $^1O_2$, we and others have observed that they are efficient quenchers of $^1O_2$ [39,40]. While the mechanism is not yet completely elucidated, it appears that association of $^1O_2$ with the fullerene surface, which has been reported by several investigators, is the initial step in deactivation of $^1O_2$ by fullerenes [41,42]. Binding of $^1O_2$ is accompanied by formation of a charge-transfer complex leading to deactivation of $^1O_2$. It has been reported that the rate of deactivation of $^1O_2$ by endohedral metallofullerenes, such as Ce@C_{82}, is similar to the diffusion controlled rate for quenching $^1O_2$ in benzene [40]. The scavenging of more reactive radicals, such as HO$^\bullet$, is expected to be mechanistically simpler, involving stochiometric addition of the radical to the fullerene [43]. Analogous scavenging of highly reactive radicals has been observed by Krusic et al. [44]. These investigators determined that one C_{60} molecule may scavenge as many as 15 benzyl radicals. This ability of certain water-soluble fullerenes to efficiently scavenge a wide range of reactive species has led to them being called “radical sponges” [45].

In addition to the mentioned molecular properties, supramolecular properties involving aggregation into nanoparticles/nanostructure may also contribute to the radical scavenging capacity of water-soluble fullerenes. It is well established that the size and structure of nanoparticles of endohedral metallofullerenes, such as Gd@C_{60}(OH)$_{22}$, affect their performance as MRI contrast agents [46]. This effect derives from the relationship between nanoparticle size, nanoparticle rotation rate in biological media and spin interactions resulting in MRI contrast enhancement [47]. However, little is known about the effects of nanoparticle size on the antioxidant and radical quenching activities of fullerenes. We determined that nanoparticles of Gd@C_{60}(OH)$_{22}$, C_{82}(OH)$_{22}$, and C_{60}(C(COOH)$_2$)$_2$ differed in average size (78 nm, 123 nm and 170 nm, respectively). A suspension of larger nanoparticles would provide smaller total surface area for interaction with the biological environment, namely, provide less reactive sites for the ROS, thus reducing the efficiency of scavenging reactive species. This factor may contribute to the relative efficiencies (i.e., Gd@C_{60}(OH)$_{22}$ ≥ C_{82}(OH)$_{22}$ > C_{60}(C(COOH)$_2$)$_2$) we note in their cytoprotection, radical scavenging and inhibition of lipid peroxidation. In addition, size may influence the distribution of nanoparticles in cells and in tissues.

We have demonstrated the biological significance of fullerenes’ antioxidant and radical scavenging activities by showing their ability to protect against oxidant-induced cytotoxicity and mitochondrial damage *in vitro*. The role of oxidative stress and damage in the etiology and progression of many diseases suggests that fullerenes may be valuable *in vivo* protective and therapeutic agents. Indeed, it has been shown that intraperitoneally injected nanoparticles of Gd@C_{60}(OH)$_{22}$ are extremely effective in shrinking tumors induced by implantation of hepatoma cells in mice [18]. This therapeutic effect was correlated with lowering markers of tumor-induced oxidative stress [19]. Gharbi *et al.* have reported that intraperitoneally pretreating mice with C_{60} resulted in reduced acute liver toxicity induced by CCl_4 [48]. This protective effect was attributed to antioxidant protection against CCl_4–induced oxidative damage. Recently, Quick *et al.* have found that an orally administered carboxyfullerene derivative protected transgenic mice, which were deficient in superoxide dismutase [49]. Protective effects included increases in lifespan, learning, and memory. Biochemical measurements demonstrated a correlation between these observed

protective effects and antioxidant protection. These studies, and others, demonstrate that the antioxidant activities of fullerenes are linked to protective and therapeutic effects. *In vitro* antioxidant and radical scavenging activities, such as those reported here, may be viewed as easily measured surrogate markers for therapeutic effects. These profiles of a fullerene's antioxidant activity should be valuable for developing highly effective fullerene derivatives for use in biomedicine.

5. Conclusion

We investigated the protective effects of three fullerene nanomaterials as the inhibitors of reactive oxygen species (antioxidants and free radical scavengers). The ESR spin trap technique provided direct in vitro evidence that the three fullerene derivatives, gadolinium endohedral metallofullerenol (Gd@C82(OH)22), fullerenol (C60(OH)22), and carboxyfullerene (C60(C(COOH)2)2), can efficiently scavenge different types of free radicals and inhibit lipid peroxidation. Both of the reactive oxygen species and the nitrogen-centered free radical were intercepted by these fullerene materials. We demonstrated in vitro by using human lung adenocarcinoma cell line A549 or rat brain capillary endothelial cell line (rBCECs) that they could reduce H2O2-induced cytotoxicity, free radical formation and mitochondrial damage. These nanomaterials have great potential in biomedical applications, for examples, gadolinium endohedral metallofullerenols can be used for both of MRI imaging and chemotherapy. The present findings provide a molecular basis of the diseases for which oxidative stress may play a key role.

Acknowledgments

This work is financially supported by the Chinese Academy of Sciences (CAS) "Hundred Talents Program" (07165111ZX), the National Basic Research Program of China (2006CB705603, 2007CB935604), the Natural Science Foundation of China (NSFC) (10525524, 20751001), and the CAS Knowledge Innovation Program. This work was also supported in part by NIH/NCRR/RCMI 2G12RR003048, NIH 5U 54CA091431, and USAMRMC W81XWH-05-1-0291 grants.

This article is not an official U.S. Food and Drug Administration (FDA) guidance or policy statement. No official support or endorsement by the U.S. FDA is intended or should be inferred.

References

1. Halliwell, B, Gutteridge, J. Free Radicals in Biology and Medicine. New York: Oxford University Press; 1989.
2. Valko M, Leibfritz D, Moncol J, Cronin MT, Mazur M, Telser J. Free radicals and antioxidants in normal physiological functions and human disease. Int J Biochem Cell Biol. 2007; 39: 44–84. [PubMed: 16978905]
3. Aust SD, Chignell CF, Bray TM, Kalyanaraman B, Mason RP. Free radicals in toxicology. Toxicol Appl Pharmacol. 1993; 120: 168–78. [PubMed: 8511786]
4. Loft S, Poulsen HE. Cancer risk and oxidative DNA damage in man. J Mol Med. 1996; 74: 297–312. [PubMed: 8862511]
5. Stadtman ER, Berlett BS. Reactive oxygen-mediated protein oxidation in aging and disease. Chem Res Toxicol. 1997; 10: 485–94. [PubMed: 9168245]
6. Toyokuni S, Okamoto K, Yodoi J, Hiai H. Persistent Oxidative Stress in Cancer. Febs Lett. 1995; 358: 1–3. [PubMed: 7821417]
7. Hileman EA, Achanta G, Huang P. Superoxide dismutase: an emerging target for cancer therapeutics. Expert Opin Ther Targets. 2001; 5: 697–710. [PubMed: 12540279]

8. Pelicano H, Carney D, Huang P. ROS stress in cancer cells and therapeutic implications. Drug Resist Updat. 2004; 7: 97–110. [PubMed: 15158766]
9. Tsai MC, Chen YH, Chiang LY. Polyhydroxylated C60, fullerenol, a novel free-radical trapper, prevented hydrogen peroxide- and cumene hydroperoxide-elicited changes in rat hippocampus in-vitro. J Pharm Pharmacol. 1997; 49: 438–45. [PubMed: 9232545]
10. Bisaglia M, Natalini B, Pellicciari R, Straface E, Malorni W, Monti D, et al. C3-fullero-tris-methanodicarboxylic acid protects cerebellar granule cells from apoptosis. J Neurochem. 2000; 74: 1197–204. [PubMed: 10693952]
11. Lai HS, Chen WJ, Chiang LY. Free radical scavenging activity of fullerenol on the ischemia-reperfusion intestine in dogs. World J Surg. 2000; 24: 450–4. [PubMed: 10706918]
12. Chueh SC, Lai MK, Lee MS, Chiang LY, Ho TI, Chen SC. Decrease of free radical level in organ perfusate by a novel water-soluble carbon-sixty, hexa(sulfobutyl)fullerenes. Transplant Proc. 1999; 31: 1976–7. [PubMed: 10455941]
13. Dugan LL, Turetsky DM, Du C, Lobner D, Wheeler M, Almli CR, et al. Carboxyfullerenes as neuroprotective agents. Proc Natl Acad Sci U S A. 1997; 94: 9434–9. [PubMed: 9256500]
14. Ali SS, Hardt JI, Quick KL, Kim-Han JS, Erlanger BF, Huang T-T, Epstein CJ, Dugan LL. A biologically effective fullerene (C_{60}) derivative with superoxide dismutase mimetic properties. Free Radic Biol Med. 2004; 37: 1191–1202. [PubMed: 15451059]
15. Dugan LL, Gabrielsen JK, Yu SP, Lin TS, Choi DW. Buckminsterfullerenol free radical scavengers reduce excitotoxic and apoptotic death of cultured cortical neurons. Neurobiol Dis. 1996; 3: 129–35. [PubMed: 9173920]
16. Chiang LY, Lu FJ, Lin JT. Free-radical scavenging activity of water-soluble fullerenols. J Chem Soc, Chem Commun. 1995. 1283–4.
17. Tang J, Xing GM, Zhao F, Yuan H, Zhao YL. Modulation of structural and electronic properties of fullerene and metallofullerenes by surface chemical modifications. J Nanosci Nanotechnol. 2007; 7: 1085–101. [PubMed: 17450881]
18. Chen CY, Xing GM, Wang JX, Zhao YL, Li B, Tang J, et al. Multihydroxylated $[Gd@C_{82}(OH)_{22}]_n$ nanoparticles: antineoplastic activity of high efficiency and low toxicity. Nano letters. 2005; 5: 2050–7. [PubMed: 16218736]
19. Wang JX, Chen CY, Li B, Yu H, Zhao YL, Sun J, et al. Antioxidative function and biodistribution of $[Gd@C_{82}(OH)_{22}]_n$ nanoparticles in tumor-bearing mice. Biochem Pharmacol. 2006; 71: 872–81. [PubMed: 16436273]
20. Yin JJ, Lao F, Meng J, Fu PP, Zhao YL, Xing GM, et al. Superior Capability of Eliminating Free Radicals by Polyhydroxylated Endohedral Metallofullerenol Optimized as ROS Species Scavenger. Mol Pharmacol. 2008; doi: 10.1124/mol.108.048348
21. Xing GM, Zhao J, Zhao YL, Tang J, Zhang B, Gao XF, et al. Influences of structural properties on stability of fullerenols. J Phys Chem B. 2004; 108: 11473–9. [PubMed: 29048898]
22. Li W, Chen CY, Ye C, Wei TT, Zhao YL, Lao F, et al. The translocation of fullerenic nanoparticles into lysosome via the pathway of clathrin-mediated endocytosis. Nanotechnology. 2008; 19. doi: 10.1088/0957-4484/19/14/145102
23. Deli MA, Abraham CS, Niwa M, Falus A. N, N-diethyl-2-[4-(phenylmethyl)phenoxy]ethanamine increases the permeability of primary mouse cerebral endothelial cell monolayers. Inflamm Res. 2003; 52 (Suppl 1) S39–40. [PubMed: 12755402]
24. Nishikawa T, Edelstein D, Du XL, Yamagishi S, Matsumura T, Kaneda Y, et al. Normalizing mitochondrial superoxide production blocks three pathways of hyperglycaemic damage. Nature. 2000; 404: 787–90. [PubMed: 10783895]
25. Basly JP, Basly I, Bernard M. ESR spectroscopy applied to the study of pharmaceuticals radiosterilization: cefoperazone. J Pharm Biomed Anal. 1998; 17: 871–5. [PubMed: 9682172]
26. Kadirov MK, Bosnjakovic A, Schlick S. Membrane-derived fluorinated radicals detected by electron spin resonance in UV-irradiated Nafion and Dow ionomers: effect of counterions and H2O2. J Phys Chem B Condens Matter Mater Surf Interfaces Biophys. 2005; 109: 7664–70. [PubMed: 16851890]

27. Yin JJ, Kramer JK, Yurawecz MP, Eynard AR, Mossoba MM, Yu L. Effects of conjugated linoleic acid (CLA) isomers on oxygen diffusion-concentration products in liposomes and phospholipid solutions. J Agric Food Chem. 2006; 54: 7287–93. [PubMed: 16968095]
28. Kusumi A, Subczynski WK, Pasenkiewicz-Gierula M, Hyde JS, Merkle H. Spin-label studies on phosphatidylcholine-cholesterol membranes: effects of alkyl chain length and unsaturation in the fluid phase. Biochim Biophys Acta. 1986; 854: 307–17. [PubMed: 3002470]
29. Burkitt MJ, Gilbert BC. The autoxidation of iron(II) in aqueous systems: the effects of iron chelation by physiological, non-physiological and therapeutic chelators on the generation of reactive oxygen species and the inducement of biomolecular damage. Free Radic Res Commun. 1991; 14: 107–23. [PubMed: 1648018]
30. Yamakoshi Y, Umezawa N, Ryu A, Arakane K, Miyata N, Goda Y, et al. Active oxygen species generated from photoexcited fullerene (C_{60}) as potential medicines: $O_2^{\bullet -}$ versus $^1O_2$. J Am Chem Soc. 2003; 125: 12803–9. [PubMed: 14558828]
31. Markovic Z, Todorovic-Markovic B, Kleut D, Nikolic N, Vranjes-Djuric S, Misirkic M, et al. The mechanism of cell-damaging reactive oxygen generation by colloidal fullerenes. Biomaterials. 2007; 28: 5437–48. [PubMed: 17884160]
32. Markovic Z, Trajkovic V. Biomedical potential of the reactive oxygen species generation and quenching by fullerenes (C(60)). Biomaterials. 2008; 29: 3561–73. [PubMed: 18534675]
33. Sayes CM, Gobin AM, Ausman KD, Mendez J, West JL, Colvin VL. Nano-C_{60} cytotoxicity is due to lipid peroxidation. Biomaterials. 2005; 26: 7587–95. [PubMed: 16005959]
34. Sayes CM, Fortner JD, Guo W, Lyon D, Boyd AM, Ausman KD, et al. The differential cytotoxicity of water-soluble fullerenes. Nano Letter. 2004; 4: 1881–7.
35. Wang L-S, Conceicao J, Changming J, Smalley RE. Threshold photodetachment of cold C^-_{60}. Chem Phys Lett. 1991; 182: 5–11.
36. Boltalina OV, Ioffe IN, Sorokin ID, Sidorov LN. Electron affinity of some endohedral lanthanide fullerenes. J Phys Chem A. 1997; 101: 9561–3.
37. Ptasiñska S, Echt O, Denifl S, Stano M, Sulzer P, Zappa F, Stamatovic A, Scheier P, Märk TD. Electron attachment to high fullerenes and to $Sc_3N@C_{80}$. J Phys Chem A. 2006; 110: 8451–56. [PubMed: 16821828]
38. Arbogast JW, Darmanyan AP, Foote CS, Rubin Y, Diedrich FN, Alvarez MM, Anz SJ, Whetten RL. Photophysical properties of C_{60}. J Phys Chem. 1991; 95: 11–2.
39. Yanagi K, Okubo S, Okazaki T, Kataura H. Endohedral metallofullerenes as strong single oxygen quenchers. Chem Phys Lett. 2007; 435: 306–10.
40. Werner H, Wohlers M, Bublak D, Blöcker J, Schlögl R. Interaction of molecular oxygen with solid C_{60}. Fullerenes, Nanotubes and Carbon Nanostructures. 1993; 1: 457–74.
41. Kopylov VB, Gavronskaya YY. Electronic and vibrational spectra of fullerenes in contact with oxygen Russian. J Gen Chem. 2001; 71: 1589–92.
42. Bensasson RV, Brettreich M, Frederiksen J, Göttinger H, Hirsch A, Land EJ, et al. Reactions of $e^-_{(aq)}$, $CO_2^{\bullet -}$, $HO^\bullet$, $O_2^{\bullet -}$, $O_2(^1\Delta_g)$ with a dendro[60]fullerene and $C_{60}[C(COOH)_2]_{(n)}$ (n=2–6). Free Radical Bio Med. 2000; 29: 26–33. [PubMed: 10962202]
43. Krusic PJ, Wasserman E, Keizer PN, Morton JR, Preston KF. Radical reactions of C_{60}. Science. 1991; 254: 1183–5. [PubMed: 17776407]
44. Xiao L, Takada H, Gan X, Miwa N. The water-soluble fullerene derivative “Radical Sponge” exerts cytoprotective action against UVA irradiation but not visible-light-catalyzed cytototoxicity in human skin keratinocytes. Bioorg Med Chem Lett. 2006; 16: 1590–5. [PubMed: 16439118]
45. Xing GM, Yuan H, He R, Gao XY, Jing L, Zhao F, et al. The Strong MRI Relaxivity of Paramagnetic Nanoparticles. J Phys Chem B. 2008; 112: 6288–6291. [PubMed: 18433163]
46. Tóth E, Bolska RD, Borel A, González Helm L, Merbach AE, Sitharaman B, Wilson LJ. Water-soluble gadofullerenes: Toward high-relaxivity, pH-responsive MRI contrast agents. J Am Chem Soc. 2004; 127: 799–805.
47. Gharbi N, Pressac M, Hadchouel M, Szwarc H, Wilson SR, Moussa F. [60]fullerene is a powerful antioxidant in vivo with no acute or subacute toxicity. Nano Lett. 2005; 5: 2578–85. [PubMed: 16351219]

48. Quick KL, Ali SS, Arch R, Xiong C, Wozniak D, Dugan LL. A carboxyfullerene SOD mimetic improves cognition and extends the lifespan of mice. Neurobiol Aging. 2008; 29: 117–28. [PubMed: 17079053]

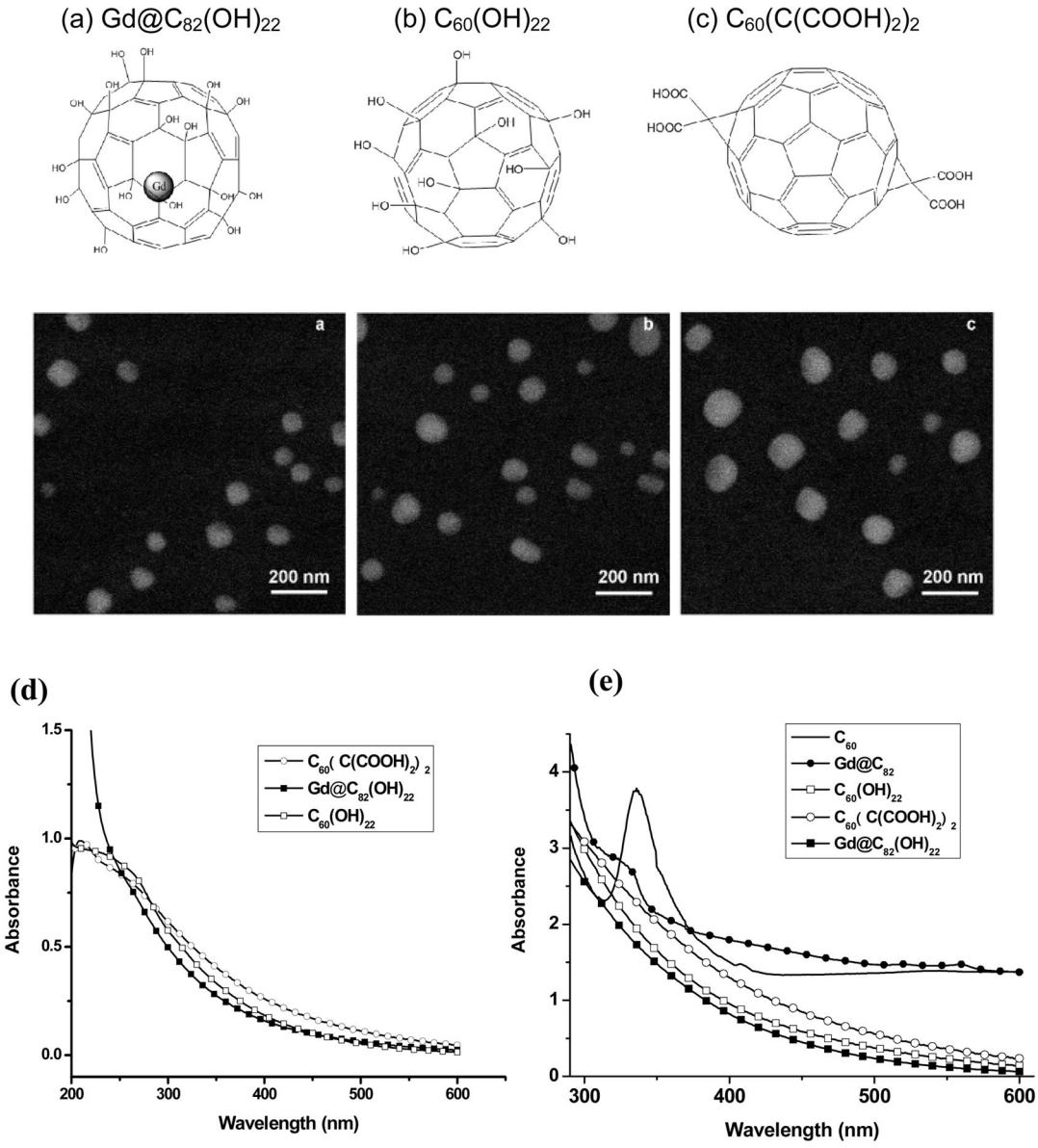

Fig. 1.

Structures and FE-SEM images of the three fullerenes: (a) Gd@$C_{82}(OH)_{22}$, (b) $C_{60}(OH)_{22,}$ (c) $C_{60}(C(COOH)_2)_2$, (d) UV-Vis absorption spectra of water-soluble fullerenes: (Gd@$C_{82}(OH)_{22}$, $C_{60}(OH)_{22,}$ and $C_{60}(C(COOH)_2)_2$ at 200 μM in PBS solution and (e) UV-Vis absorption spectra of Gd@$C_{82}(OH)_{22}$, $C_{60}(OH)_{22}$, $C_{60}(C(COOH)_2)_{2,}$ Gd@C_{82}, and $C_{60.}$ Gd@C_{82} and C_{60} were prepared at 1 mM in toluene solutions.

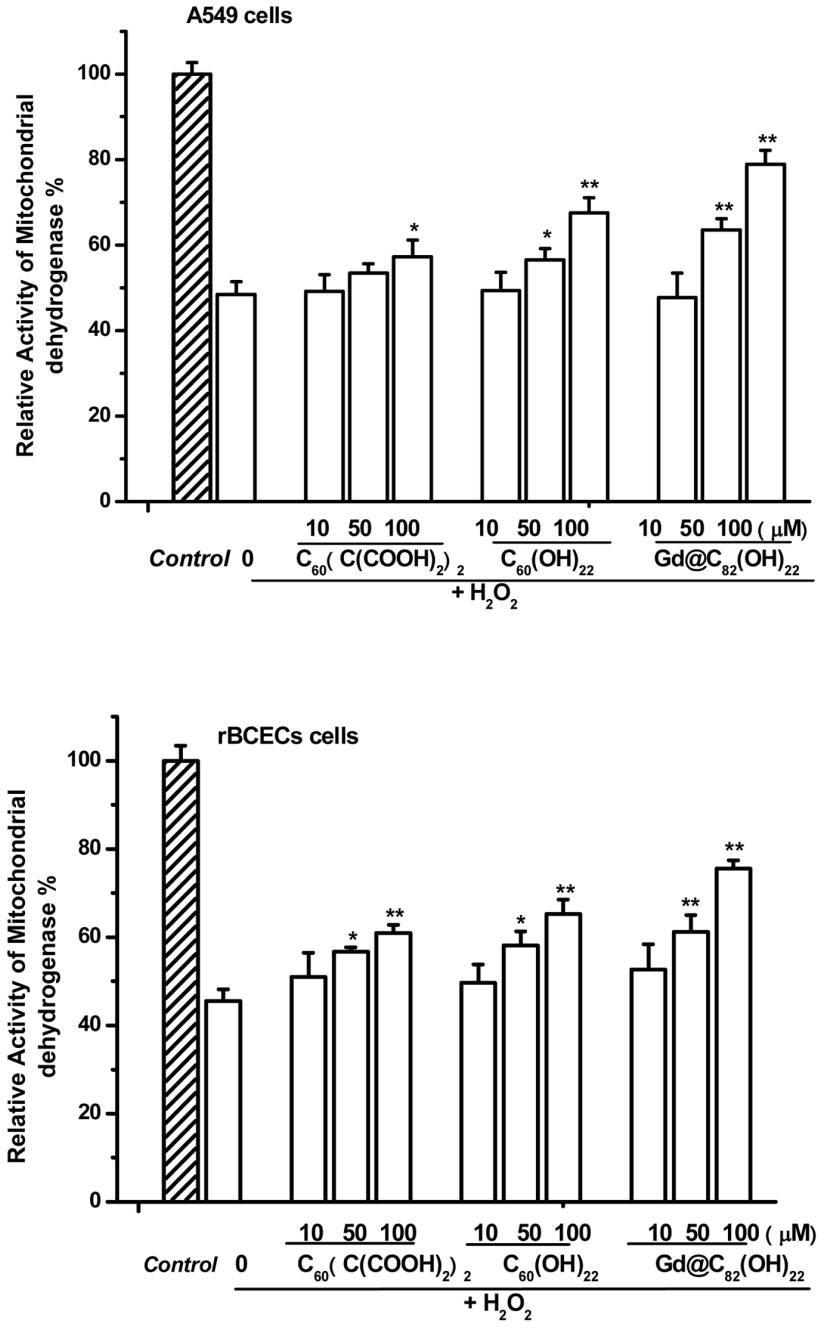

Fig. 2.

Protective effects of three fullerene derivatives: $Gd@C_{82}(OH)_{22}$, $C_{60}(OH)_{22}$, and $C_{60}(C(COOH)_2)_2$ against H_2O_2-induced damage in A549 cells and rBCECs cells. The cells were treated with 10–100 μM fullerene derivatives before incubation with 50 μM H_2O_2. **P*<0.05 and ***P*<0.01 vs. H_2O_2-treated control.

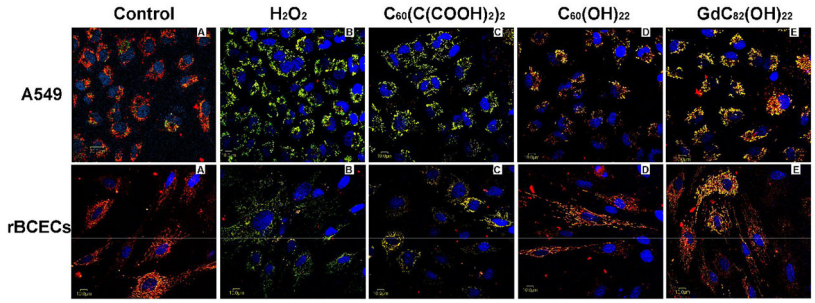

Fig. 3.

The protective effects three fullerene derivatives Gd@$C_{82}(OH)_{22}$, $C_{60}(OH)_{22}$, and $C_{60}(C(COOH)_2)_2$. against H_2O_2-induced mitochondrial damage in A549 cells, and rBCECs cells. The cells were treated with 100 μM fullerene derivatives before incubation with 50 μM H_2O_2. Aggregation of the dye, JC-1, seen as red fluorescence, indicates integrity of the mitochondrial membrane.

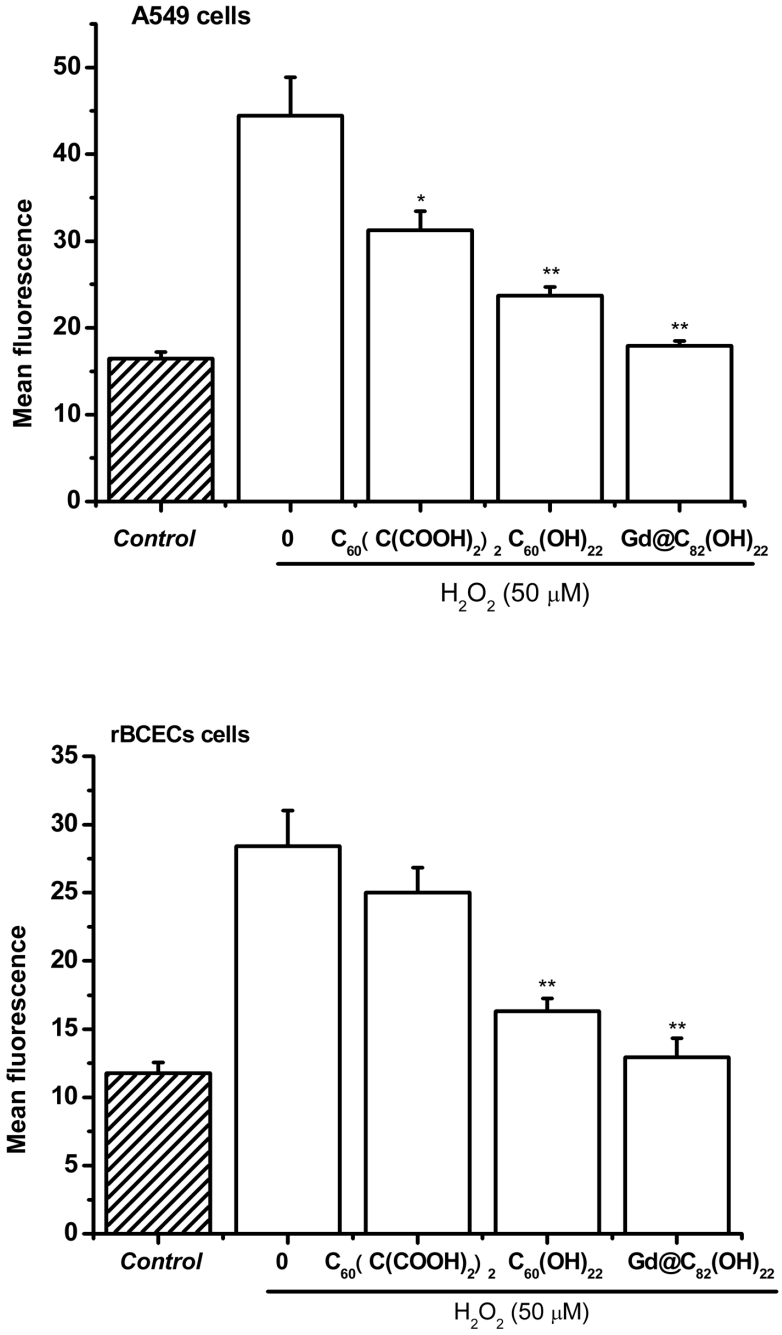

Fig. 4.

Protective effects of fullerene derivatives, $Gd@C_{82}(OH)_{22}$, $C_{60}(OH)_{22}$, and $C_{60}(C(COOH)_2)_2$, against H_2O_2-induced ROS generation in A549 cells or rBCECs cells. The cells were treated with 100 μM fullerene derivatives before incubation with 50 μM H_2O_2. *P<0.05 and **P<0.01 vs. H_2O_2-treated control.

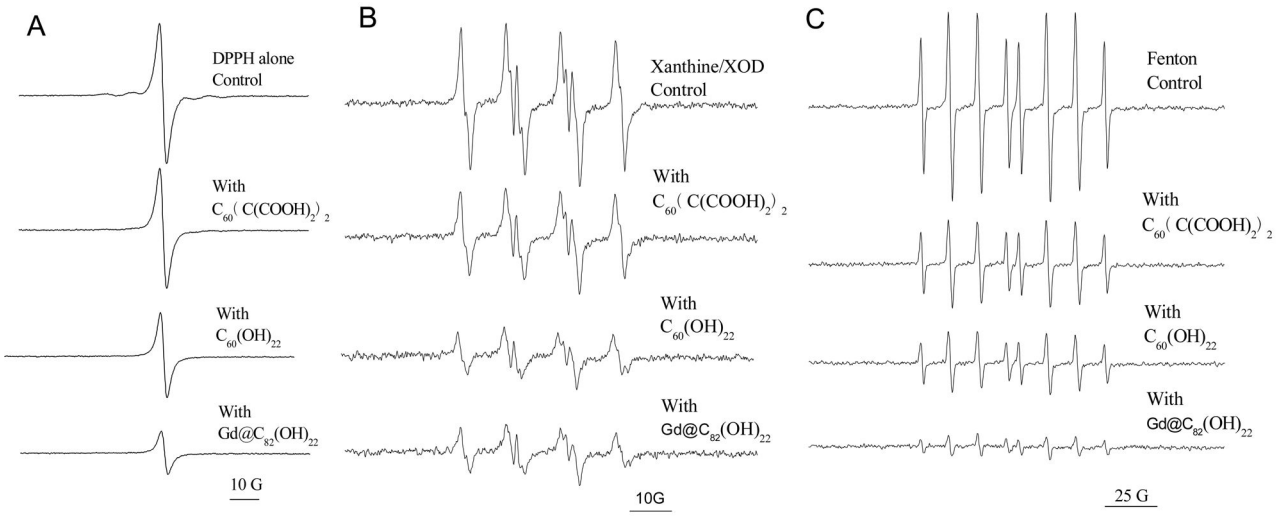

Fig. 5.

Scavenging of DPPH• (A), superoxide radical anions (B) and hydroxyl radicals (C) by three fullerenes, $C_{60}(C(COOH)_2)_2$, $C_{60}(OH)_{22}$, and $Gd@C_{82}(OH)_{22}$. For DPPH• (A), samples contained 100 μM fullerenes, and 0.1 mM DPPH in 20% ethanol; and ESR spectra were recorded 5 min after sample mixing at room temperature. For superoxide radical anions (B), samples contained 20 mM BMPO, with and without 150 μM fullerenes, mixed with 1 mM xanthine, 0.05 mM DTPA and 0.1 unit/ml xanthine oxidase. Data were recorded 1.5 min after addition of XOD at room temperature. For hydroxyl radicals (C), samples contained 0. 5 mM DEPMPO, with and without 100 μM fullerenes, 0.2 mM H_2O_2 and 0.02 mM Fe^{2+}. Data were recorded 5 min after addition of Fe^{2+} at room temperature.

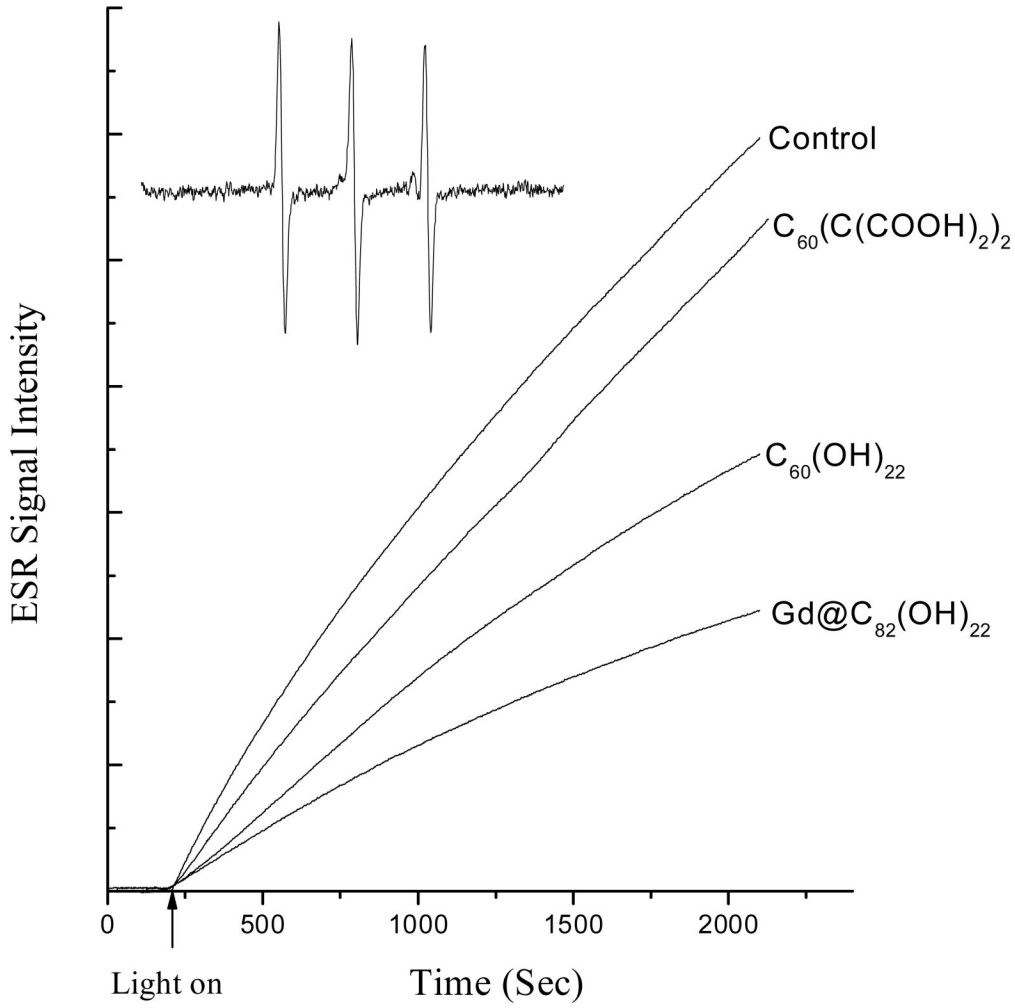

Fig. 6.

Time dependence of ESR signal for the formation of TEMP-$^1O_2$ adducts. $^1O_2$ was generated by irradiation of Rose Bengal with visible light (560 nm) at ambient temperature. Samples contained 10 mM TEMP and 0.1 mM Rose Bengal, with and without a fullerene derivative (200 μM). The inset is the ESR spectrum of the TEMP-$^1O_2$ adduct observed in all the cases. The time scans of ESR signal intensity were obtained with fixed field position (the peak position of the center line of ESR spectrum), 15 mW microwave power and 1 G field modulation.

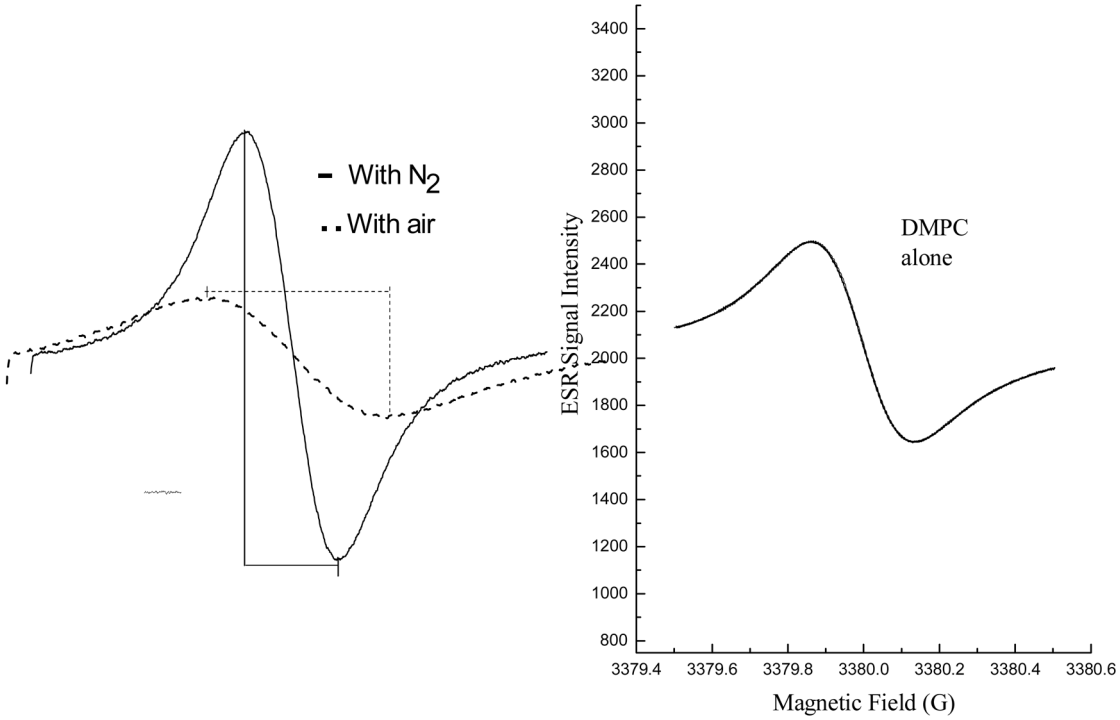

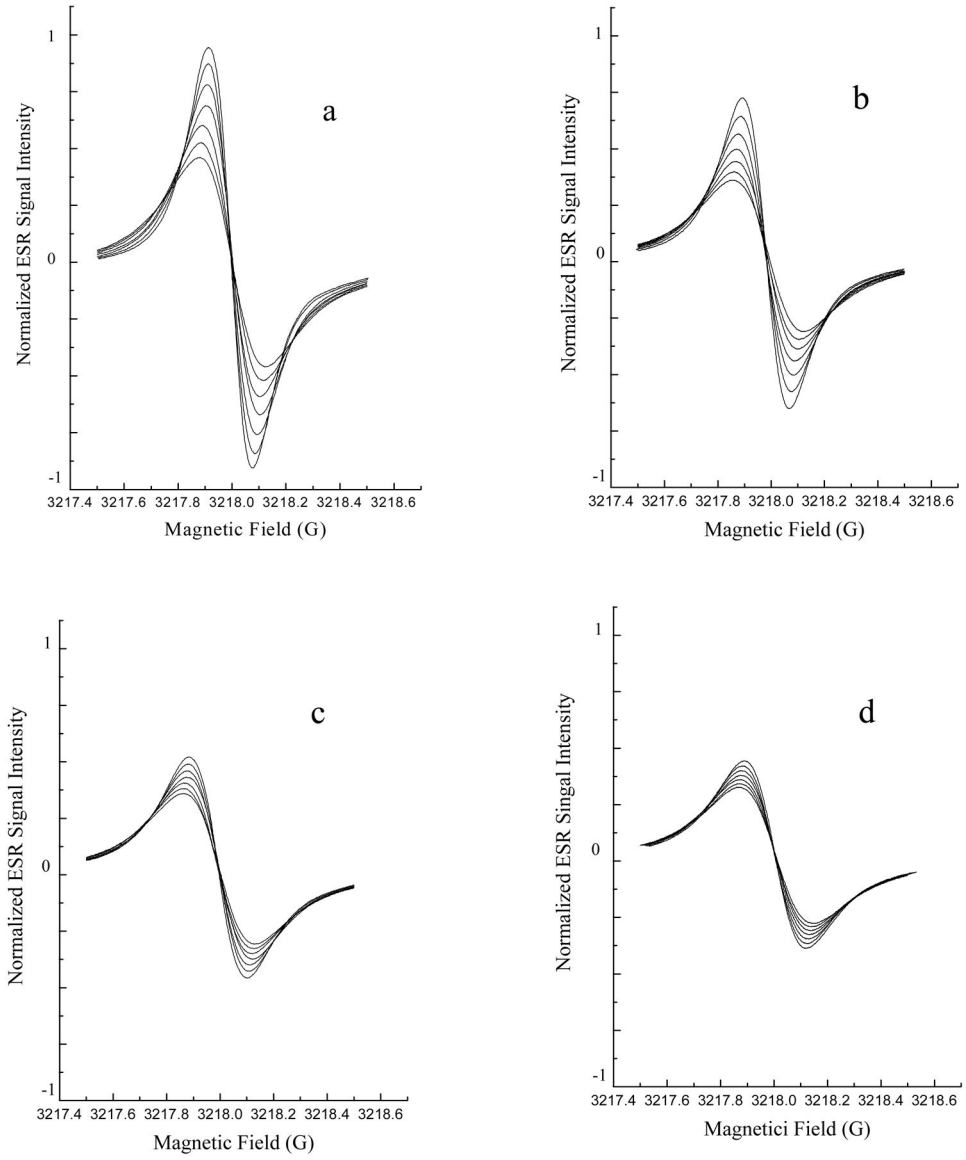

Fig. 7. Effect of fullerene derivatives on lipid peroxidation in liposomes

Fig. 7A. Oxygen consumption is measured in a closed chamber using liposome suspensions and the spin label ^{15}N-Tempone mixed with a free radical initiator such as AAPH. The left panel shows ESR spectra of the scans of the low field line of ^{15}N-Tempone in a nitrogen atmosphere (solid line) or air-saturated (broken line) aqueous solutions. The presence of oxygen results in a broader and less intense ESR signal for the spin probe. Lipid peroxidation was measured in the control experiment (left panel) with saturated lipid, DMPC, where there is no oxygen consumption because no lipid peroxidation involved. Spectra were recorded at 37°C; 0.5 mW microwave power, 0.05 G modulation amplitude, and 1 G scanning range.

Fig. 7B. Lipid peroxidation was inhibited by fullerene nanoparticles.

Lipid peroxidation was assessed using ESR oximetry. The samples contained liposomes (30 mg/mL egg phosphatidylcholine) and 0.1 mM ^{15}N-Tempone (PD) spin label. Fullerene

nanoparticles were also added to some samples (Panel A, no fullerene; Panel B, 300 μM $C_{60}(C(COOH)_2)_2$; Panel C, 200 μM $C_{60}(OH)_{20}$; Panel D 200 μM $Gd@C_{82}(OH)_{22}$). Lipid peroxidation was initiated by adding 25 mM AAPH. After the sample was sealed in a capillary, the ESR spectrum was recorded 7 times at 4 min intervals with a Varian E-109 X-band spectrometer with a variable temperature controller accessory as described in the Experimental Section. Signals were obtained with 0.5 mW incident microwave power and with 0.05 G field modulation at 37°C. The progressive increases in peak to peak signal intensity (and accompanying progressive narrowing of line width) in each panel are due to time-dependant oxygen consumption resulting from lipid peroxidation. The inhibitory effects of fullerene nanoparticles on lipid peroxidation may be seen as smaller changes in peak to peak signal intensities seen in panels B, C and D compared to panel A.

Table 1

Comparison of protective effects of three fullerene derivatives $Gd@C_{82}(OH)_{22}$, $C_{60}(OH)_{22}$, and $C_{60}(C(COOH)_2)_2$ on H_2O_2-induced cytotoxcity and intracellular ROS generation in A549 cells or rBCECs cells.

Percentage of inhibition (%)	Cell viability		Total ROS Level	
	A549	rBCECs	A549	rBCECs
$Gd@C_{82}(OH)_{22}$	59.1±3.3	54.1±1.9	94.6±2.6	93. 5±3.4
$C_{60}(OH)_{22}$	37.1±3.5	35.5±3.3	74.1±3.5	72.7±2.9
$C_{60}(C(COOH)_2)_2$	17.2±3.8	27.8±1.9	47.2±2.2	20.4±1.8

Note: For measuring effects on cell viability, the cells were treated with 100 μmol/ml fullerene derivatives before incubation with 50 μM H_2O_2. Cell viability was assessed by measurement of mitochondrial dehydrogenase activity. For measurement of intracellular ROS, the same conditions for incubation with H_2O_2 were used. Levels of intracellular ROS were determined by flow cytometry.

Table 2

Scavenging of DPPH$^{\bullet}$ radical, superoxide radical anion, singlet oxygen, hydroxyl radical, and inhibition of lipid peroxidation by three fullerene derivatives, $C_{60}(C(COOH)_2)_2$, $C_{60}(OH)_{22}$, and $Gd@C_{82}(OH)_{22}$.

Percentage of Scavenging or Inhibition (%)	DPPH$^{\bullet}$	$O_2^{\bullet -}$	$^1O_2$	OH$^{\bullet}$	Lipid peroxidation
$Gd@C_{82}(OH)_{22}$	75	65.8	58.2	88.1	56.1
$C_{60}(OH)_{22}$	45.5	65.8	38.2	66.7	44.6
$C_{60}(C(COOH)_2)_2$	13.6	31.6	9.1	54.8	39.2